[12]P. Resibois, Phys. Rev. 138, B281 (1965).
[13]V. Heine, P. Nozières, and J. W. Wilkins, Phil. Mag. 13, 741 (1966).
[14]This possibility has been suggested to the authors by J. Friedel and J. R. Schrieffer.
[15]R. E. Prange, Phys. Letters 12, 181 (1964).
[16]W. F. Brinkman and T. M. Rice, Phys. Rev. B 4, 1566 (1971).

PHYSICAL REVIEW B VOLUME 5, NUMBER 11 1 JUNE 1972

# Critical-Field Curve of Superconducting Lead†

G. Chanin and J. P. Torre
*Service d'Aéronomie du Centre National de la Recherche Scientifique, Verrières-le-Buisson, France*
(Received 20 January 1972)

The critical field of pure monocrystalline lead has been measured throughout its range. A vibrating phase-boundary technique was used, permitting continuous observation of the boundary between the normal and superconducting phases within the sample. Because of the coexistence of both phases at all times, supercooling and superheating effects are avoided. Departures from thermodynamic equilibrium are small, as is indicated by the very weak hysteresis (as low as several parts in 10 000). The deviation curve is strongly positive, as expected for strong-coupling superconductors. The measured values of the usual superconductive parameters are $T_c = (7.195 \pm 0.006)$ °K, $H_0 = 803.4 \pm 0.3$ Oe, $dH_c/dT|_{T_c} = 237.3 \pm 1.1$ Oe/°K.

## I. INTRODUCTION

The very low Debye temperature (~ 96 °K) and high critical temperature (7.2 °K) of lead class it as an extreme strong-coupling superconductor. In contrast to the negative values for the deviation from parabolic behavior that characterize the critical field curves of the weak-coupling superconductors, lead shows a positive deviation curve. While the Bardeen-Cooper-Schrieffer[1] (BCS) theory of superconductivity is in very close agreement with the deviation curves of weak-coupling superconductors such as aluminum,[2] intermediate- and strong-coupling superconductors remain difficult to treat theoretically. An extension of the BCS theory shows promise of handling this class of metals.[3]

The critical field curve of lead merits study because, in addition to its being a strong-coupling superconductor, no recent measurements have been made which determine the curve throughout its range, obtaining both $H_0$ and $T_c$ for the same specimen. Since calorimetric measurements of the heat capacity are dominated by the lattice contribution, the electronic heat capacity cannot be accurately determined except from thermodynamic analysis of the critical field curve.

## II. EXPERIMENT

### A. Sample

The sample, a cylindrical single crystal of lead 2 mm in diam, 12 cm long, and nominal purity 99.999%, was supplied by Monocrystals Inc. of Cleveland, Ohio. It was selected from among three specimens of different manufacture for its surface regularity and smoothness. A chemical etch confirmed its single-crystal structure and freedom from surface defects. The sample quality may best be judged from its residual-resistance ratio. After the completion of the magnetic measurements, its electrical resistance was measured at room temperature and at 4.2 °K. For the latter, a series of resistance values at different field strengths from 560 to 780 Oe were extrapolated to zero field in order to obtain the normal-state resistance corrected for magnetoresistance effects. The residual-resistance ratio thus obtained was $R_{273}/R_{4.2} = 15\,000$ indicating a very high sample purity.

### B. Apparatus

The cryogenic apparatus was designed to permit operation in three temperature ranges: $He^3$, $He^4$, and above 4.2 °K, without disassembly or warmup of the sample. The double-walled cryostat of Fig. 1 was mounted within conventional glass Dewars for liquid nitrogen and liquid helium. All materials used were nonmagnetic and nonsuperconductive in order to avoid perturbing the magnetic field near the sample. Two pairs of Helmholtz coils surrounding the outer Dewar were used to cancel the horizontal and vertical components of the Earth's magnetic field to less than $10^{-2}$ Oe over the region occupied by the sample. Within the liquid-nitrogen Dewar a solenoid provided the magnetic field for the superconductive transition. Its

power supply, programmable for linear scans in both directions, was stable to 10 ppm. A pumping system incorporating a diaphragm pressure regulator allowed temperatures in the inner glass Dewar to be stabilized at any value between 1.4 and 4.2 °K.

The lead crystal, supported co-axially within the measurement coils, was mounted in the oxygen-free-high-conductivity (OFHC) copper-sample cavity as in Fig. 1. Thermometers (two carbon resistors and two germanium thermometers) and a heater were epoxy cemented to the inner wall of this cavity. The cavity was sealed at the bottom with a gold gasket while the electrical leads left via a hermetic epoxy seal.[4] Helium gas could be bled into the cavity through a capillary tube to promote thermal exchange between the sample, thermometers, heater, and cavity walls. The capillary tube also allowed readout of the gas pressure when the gas thermometer mode of operation was used. Two small reservoirs are fitted into the upper portion of the container: one for a $He^3$ refrigerant bath, the other for $He^3$ or $He^4$ vapor-pressure measurements. The tubes to these reservoirs are optically baffled to prevent descending thermal radiation from producing temperature gradients. A simple one-shot $He^3$ system circulated the $He^3$ gas between cryostat and reservoir and allowed temperatures between 0.3 and 1.4 °K to be maintained and measured.

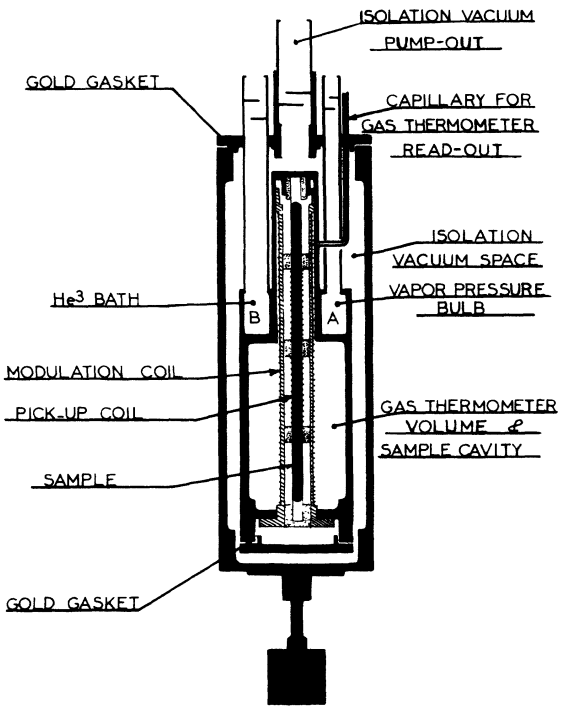


FIG. 1. Liquid-helium portion of the apparatus. The concentric liquid-helium and liquid-nitrogen Dewars and the liquid-nitrogen-cooled solenoid are omitted for clarity.

A concentric brass tube forms the outer envelope of the cryostat. A gold-gasket seal to the upper flange and a pumping tube from the flange to an outside diffusion pump allows a high vacuum for thermal isolation.

A three-wire Wheatstone bridge was used to read the resistance thermometers. Servo-regulation of the temperature was obtained by amplifying the unbalance voltage of the bridge and using it to modify the electrical power dissipated by a heater located in the sample cavity or in the helium bath.

### C. Thermometry between 0.3 and 4.2 °K

The $He^3$-temperature region was covered by pumping on the $He^3$ bath while measuring the vapor pressure of $He^3$ in the separate vapor-pressure compartment using a dial manometer or a McLeod gauge. The $T^{62}$ $He^3$ vapor-pressure scale[5] was used for the determination of the absolute temperature. During these measurements, superfluid liquid $He^4$ filled the sample cavity to assure thermal contact with the $He^3$ bath and the vacuum isolation space was maintained at high vacuum. Servo-regulation of the temperature to $30\times10^{-6}$ °K was possible with the thermometer and heater in the sample cavity.

The $He^4$ range was obtained with condensed $He^4$ in the vapor-pressure compartments, in the sample cavity, and in place of the vacuum isolation. The heater in the sample cavity was not used in order to avoid heating it above the bath temperature: Since this might result in an error in the vapor-pressure reading because of refluxing in the read-out tube where it passed through the colder $He^4$ bath, we chose instead to heat the bath itself by a heater at the bottom of the glass helium Dewar. Temperature regulation in this region was to about $200\times10^{-6}$ °K. The $T^{58}$ $He^4$ vapor-pressure scale[6] was employed.

### D. Thermometry between 4.2 and 7.2 °K

For each value of thermometer resistance corresponding to a datum point, gas thermometry was used to obtain the corresponding absolute temperature without warmup of the thermometers. In this mode of operation the vacuum isolation was continuously pumped to less than $10^{-7}$ Torr. Helium gas was introduced into the sample cavity, and its pressure read out through the $\frac{3}{10}$-mm-i.d. stainless-steel capillary tube. The pressure-measuring device was a Texas Instruments fused-quartz pressure gauge, providing, to a sufficiently high approximation, constant volume readings. To avoid errors from the diffusion of helium gas through the quartz walls of the Bourdon element, all measurements of a calibration run were completed within several hours. The total immersion of thermometers, heater, and sample within the gas thermom-

eter assures the highest-possible thermal contact between them and the gas. Typical servo-regulation in this region was to $10\times10^{-6}$ °K.

The equation of state of a nonideal gas is usually written

$$PV/T(1+B/v)=nR\,, \tag{1}$$

where $P$ is the pressure, $V$ and $T$ are the volume and temperature, respectively, $B$ is the second virial coefficient, $v$ is the molar volume, $n$ is the number of moles of gas in the system, and $R$ is the universal gas constant. For the case where the system consists of the sample-cavity volume (61.5 cm) at low temperature, a smaller distribution of gas in the capillary tube at intermediate temperatures, and the volume within the pressure gauge at room temperature, the system will be described by

$$\frac{PV}{T(1+B/v)}+P\int\frac{dV}{T_i}=nR\,, \tag{2}$$

where $V$ and $T$ refer to the temperature and volume in the sample cavity, and the integral is the contribution from the intermediate- and room-temperature parts of the apparatus at local temperatures $T_i$.

Defining

$$S\equiv\frac{T}{V}\int\frac{dV}{T_i} \tag{3}$$

as the "dead"-volume correction and noting that the molar volume may be expressed as $v=V/n$, the equation to be satisfied becomes

$$\frac{P}{T}=R\left(\frac{n}{V}\right)\left[1+B\left(\frac{n}{V}\right)-S+S^2-2SB\left(\frac{n}{V}\right)+\cdots\right]. \tag{4}$$

Assuming the volume $V$ to be independent of temperature for the temperature range under consideration (because the temperature coefficient of expansion of copper is negligibly small in this range), the temperature enters in the right-hand side of this equation in the values of $B$ and $S$. The computation of $S$ must, in addition to $T$, take into account the temperature of the room and the length of capillary tube immersed in liquid helium. The second virial coefficient uses the adopted values of Keesom[7] in the form of an empirical formula.

The pressure $P$, measured at the room-temperature end of the capillary, requires correction for thermomolecular effects. The treatment of Sydoriak and Roberts[8] using the Weber-Schmidt equation was applied in order to obtain the pressure in the sample cavity as a function of temperature.

The determination of $n/V$ in Eq. (4) required a least-squares fit to calibration data in the range 3.3–4.2 °K.

The temperatures at the data points above 4.2 °K were then computer determined by an iterative fit of Eq. (4) until the resultant temperatures changed less than 1 m °K. Two gas-thermometer runs were made at different initial filling pressures. Each datum point is the mean of the two values obtained. We estimate the absolute uncertainty in temperature from all causes (except the $He^4$ vapor-pressure scale) to be not greater than 6 m °K at 7 °K and less at lower temperatures.

### E. Detection of Superconductive Transitions

A complete description of the technique for the creation and detection of the phase boundary between normal and superconducting regions has already been given elsewhere.[2] A brief description of the technique follows: The sample is located in a magnetic field, parallel to its axis and of gradient 0.05% of applied field/cm. When the field is adjusted to a value of $H_c$ at the midpoint of the sample, a phase boundary appears at this point, splitting the sample into superconductive and normal phases. A small ($<10^{-2}$-Oe) ac field at 2.3 Hz causes the phase boundary to move back and forth along the sample. The movement is detected by two pickup coils, in series opposition, along the sample. Assuming the boundary to be neither "pinned" nor damped, its position at any instant is that where the local-field value equals $H_c$. This results in an induced voltage in the pickup coil of approximately

$$V=\left(\frac{nA}{\beta}\right)\frac{dH}{dt}\bigg|_{\text{Mod}}\,, \tag{5}$$

where $n$ is the number of turns/cm of the pickup coil, $A$ is the cross-sectional area of the sample, $\beta\equiv(1/H)\,\text{grad}H$, and $dH/dt\,|_{\text{Mod}}$ refers to the ac field generated by the modulation coil.

As the phase boundary moves along the sample in response to the slowly increasing ($\sim10^{-2}$ Oe/min) magnetic field, the induced signal voltage will change phase with respect to the modulation field when the boundary leaves the part of the sample surrounded by the first coil to enter that of the second. Synchronous detection of this induced voltage with respect to the modulation field as a reference converts this phase change to a change in polarity. The passage of the boundary through the region between the two coils is thus revealed and the critical field is the instantaneous field value at this point. Hysteresis measurements are obtained by slowly decreasing the field until this same point is reached.

The chart recording of Fig. 2 shows how the transition is observed. The linear trace at the right is proportional to the applied field at the point between the two pickup coils. The initial deviation of the signal trace from zero corresponds to the appearance of the phase boundary within the first

TABLE I. Critical-field data.

| $T$ (°K) | $H_c$ (Oe) | Hysteresis (%) |
|---|---|---|
| 0.474 ± 0.005 | 800.31 ± 0.05 | |
| 0.542 ± 0.004 | 799.05 ± 0.05 | |
| 0.586 ± 0.002 | 798.49 ± 0.05 | |
| 0.670 ± 0.002 | 797.00 ± 0.05 | 0.32 |
| 0.755 ± 0.002 | 795.27 ± 0.05 | |
| 0.903 ± 0.001 | 792.47 ± 0.05 | 0.32 |
| 1.019 ± 0.001 | 789.11 ± 0.05 | |
| 1.198 ± 0.001 | 783.79 ± 0.05 | 0.31 |
| 1.205 ± 0.001 | 783.35 ± 0.05 | |
| 1.212 ± 0.001 | 783.25 ± 0.05 | |
| 1.349 ± 0.001 | 778.25 ± 0.05 | |
| 1.449 ± 0.005 | 774.50 ± 0.05 | |
| 1.645 ± 0.004 | 765.97 ± 0.05 | |
| 1.794 ± 0.003 | 759.14 ± 0.05 | 0.19 |
| 2.029 ± 0.002 | 746.27 ± 0.05 | |
| 2.277 ± 0.001 | 731.11 ± 0.05 | |
| 2.493 ± 0.001 | 716.34 ± 0.05 | 0.10 |
| 2.496 ± 0.001 | 716.34 ± 0.05 | |
| 2.687 ± 0.001 | 702.07 ± 0.05 | |
| 2.849 ± 0.001 | 689.04 ± 0.05 | |
| 3.057 ± 0.001 | 670.85 ± 0.05 | |
| 3.218 ± 0.001 | 655.79 ± 0.05 | 0.06 |
| 3.513 ± 0.001 | 626.05 ± 0.05 | |
| 3.515 ± 0.001 | 625.77 ± 0.05 | |
| 3.529 ± 0.001 | 624.65 ± 0.05 | |
| 3.640 ± 0.001 | 612.38 ± 0.05 | |
| 3.670 ± 0.001 | 609.32 ± 0.05 | 0.04 |
| 3.804 ± 0.001 | 594.10 ± 0.05 | |
| 3.804 ± 0.001 | 594.07 ± 0.05 | |
| 3.940 ± 0.001 | 577.98 ± 0.05 | 0.03 |
| 4.065 ± 0.001 | 562.79 ± 0.05 | |
| 4.190 ± 0.001 | 547.04 ± 0.05 | |
| 4.206 ± 0.001 | 544.55 ± 0.05 | 0.04 |
| 4.348 ± 0.002 | 526.13 ± 0.05 | |
| 4.348 ± 0.002 | 526.46 ± 0.05 | |
| 4.478 ± 0.003 | 508.72 ± 0.05 | 0.04 |
| 4.478 ± 0.003 | 508.55 ± 0.05 | |
| 4.625 ± 0.003 | 487.98 ± 0.05 | |
| 4.625 ± 0.003 | 487.92 ± 0.05 | |
| 4.753 ± 0.003 | 469.62 ± 0.05 | |
| 4.753 ± 0.003 | 469.26 ± 0.05 | |
| 4.845 ± 0.003 | 455.68 ± 0.05 | 0.04 |
| 4.845 ± 0.003 | 456.38 ± 0.05 | |
| 4.946 ± 0.004 | 440.34 ± 0.06 | |
| 4.946 ± 0.004 | 440.71 ± 0.05 | |
| 5.117 ± 0.004 | 413.56 ± 0.05 | |
| 5.117 ± 0.004 | 413.79 ± 0.05 | |
| 5.314 ± 0.004 | 381.51 ± 0.05 | 0.05 |
| 5.314 ± 0.004 | 381.29 ± 0.05 | |
| 5.461 ± 0.004 | 355.66 ± 0.05 | |
| 5.461 ± 0.005 | 355.96 ± 0.05 | |
| 5.632 ± 0.005 | 326.08 ± 0.05 | |
| 5.632 ± 0.005 | 326.23 ± 0.05 | |
| 5.769 ± 0.005 | 300.66 ± 0.05 | 0.05 |
| 5.926 ± 0.005 | 271.82 ± 0.06 | |
| 6.036 ± 0.005 | 250.46 ± 0.06 | |
| 6.130 ± 0.005 | 231.83 ± 0.06 | |
| 6.205 ± 0.005 | 216.96 ± 0.06 | |
| 6.283 ± 0.005 | 201.13 ± 0.06 | |
| 6.366 ± 0.005 | 184.39 ± 0.06 | 0.07 |
| 6.423 ± 0.005 | 172.64 ± 0.06 | |

TABLE I. (*Continued*)

| $T$ (°K) | $H_c$ (Oe) | Hysteresis (%) |
|---|---|---|
| 6.495 ± 0.006 | 157.20 ± 0.02 | |
| 6.586 ± 0.006 | 137.64 ± 0.02 | |
| 6.685 ± 0.006 | 116.66 ± 0.02 | |
| 6.769 ± 0.006 | 98.19 ± 0.02 | 0.08 |
| 6.837 ± 0.006 | 82.60 ± 0.02 | |
| 6.910 ± 0.006 | 66.25 ± 0.02 | |
| 6.985 ± 0.006 | 49.07 ± 0.01 | |
| 7.064 ± 0.006 | 31.08 ± 0.01 | |
| 7.103 ± 0.006 | 21.72 ± 0.01 | |
| 7.103 ± 0.006 | 21.69 ± 0.01 | 0.1 |
| 7.123 ± 0.006 | 17.04 ± 0.01 | |
| 7.123 ± 0.006 | 17.07 ± 0.01 | |
| 7.143 ± 0.006 | 12.24 ± 0.01 | |
| 7.154 ± 0.006 | 9.85 ± 0.01 | |
| 7.165 ± 0.006 | 7.29 ± 0.01 | 0.3 |
| 7.175 ± 0.006 | 4.87 ± 0.01 | |
| 7.185 ± 0.006 | 2.42 ± 0.005 | |
| 7.185 ± 0.006 | 2.38 ± 0.005 | |
| 7.187 ± 0.006 | 1.895 ± 0.005 | |
| 7.187 ± 0.006 | 1.90 ± 0.005 | |

pickup coil. Its change in polarity corresponds to the passage of the boundary into the second coil; the corresponding value of the applied field is taken

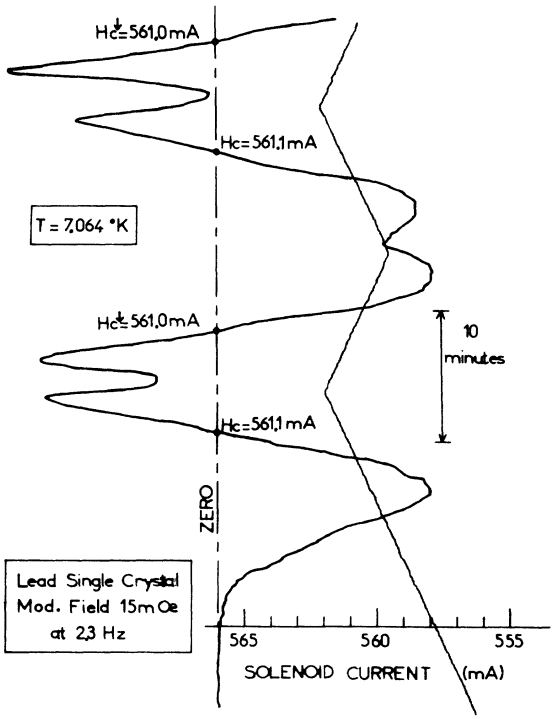


FIG. 2. Example of a data recording. Two transitions from the superconducting to the normal state and return are shown, and the corresponding solenoid currents (proportional to the magnetic field) are indicated. The hysteresis observable here is less than the average for this temperature region (see Table I).

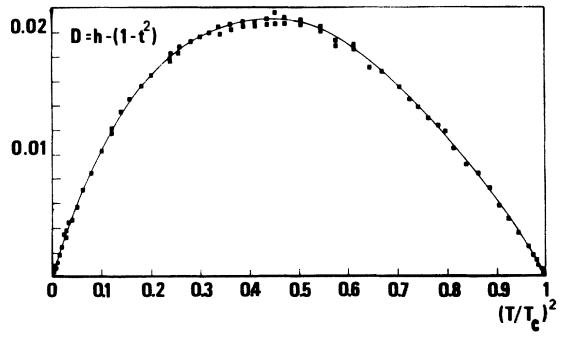


FIG. 3. Deviation from parabolic temperature dependence vs $(T/T_c)^2$. Data points are represented by the black squares.

as the critical field $H_c$ for the transition from the superconducting to the normal state. Upon reversing the field scan, the signal trace also reverses itself and the critical field for the transition from the normal to the superconducting state $H_{c'}$ is that value of field corresponding to the second crossing of the zero base line. The percent hysteresis may be expressed by

$$\% \text{ hysteresis} \equiv (H_c - H_{c'})/H_c \times 100 . \tag{6}$$

## III. RESULTS

The critical field measurements obtained by an uninterrupted series of measurements on our sample are summarized in Table I. These measurements extended over a 2-month period during which the sample and thermometers were maintained at liquid-helium temperatures. For experimental convenience, the data-taking sequence was not completely random except within each of the three general temperature ranges. The observed hysteresis of the transition is also given at several representative temperatures.

Supercooling phenomena occurred readily if the field was allowed to increase to the point that the phase boundary left the sample and it became entirely normal. Upon reduction of the field, the magnetic flux would be suddenly expelled from the sample at field values much lower (~10%) than the critical field. As there would be no orderly movement of a phase boundary through the sample, the chart recording would reveal only a brief and extremely large pulse. To avoid supercooling, in the data points of Table I, the field scan was reversed just after the phase boundary entered the second pickup coil so that both phases were always present in the sample. Under these conditions no supercooling was ever observed. Superheating phenomena were not observed since the stronger field at the extremities of the sample caused by edge effects would cause these regions to become normal even with applied fields slightly below $H_c$.

From the data of Table I, the critical temperature $T_c$ and the critical field $H_c$ were obtained by graphical extrapolation of the curve $H_c$ vs $T^2$. These values are $T_c = (7.195 \pm 0.006\ ^\circ\text{K}$, $H_0 = 803.4 \pm 0.3$ Oe. The slope of the curve at $T_c$ yields

$$\left.\frac{dH_c}{dT}\right|_{T_c} = 2T_c \left.\frac{dH_c}{dT^2}\right|_{T_c} = -237.3 \pm 1.1 \text{ Oe}/^\circ\text{K}. \tag{7}$$

From the above values, we may trace the curve of the deviation from parabolic behavior:

$$D \equiv H_c/H_0 - [1 - (T/T_c)^2]. \tag{8}$$

The curve of $D$ vs $t^2$, where $t \equiv T/T_c$, is shown in Fig. 3.

From the deviation curve it is possible by successive differentiations to obtain the entropy, the latent-heat, and the heat-capacity curves. Note that

$$\Delta S = S_N - S_S = -\frac{V}{8\pi}\frac{dH_c^2}{dT} \tag{9}$$

and

$$\Delta S = \frac{VH_0^2}{2\pi T_c} ht\left(1 - \frac{dD}{dt^2}\right), \tag{10}$$

from which the latent heat $L = T\Delta S$ may also be obtained. These curves are presented in Figs. 4 and 5. The difference in heat capacities $\Delta C = d\Delta S/dT$ is

$$\Delta C = C_{es} - C_{en} = \frac{T}{T_c}\frac{d\Delta S}{dt},$$

and this curve is presented in Fig. 6. The value at $T_c$ is

$$\Delta C_{T_c} = 59.9 \pm 0.6 \text{ mJ/mole } ^\circ\text{K}. \tag{11}$$

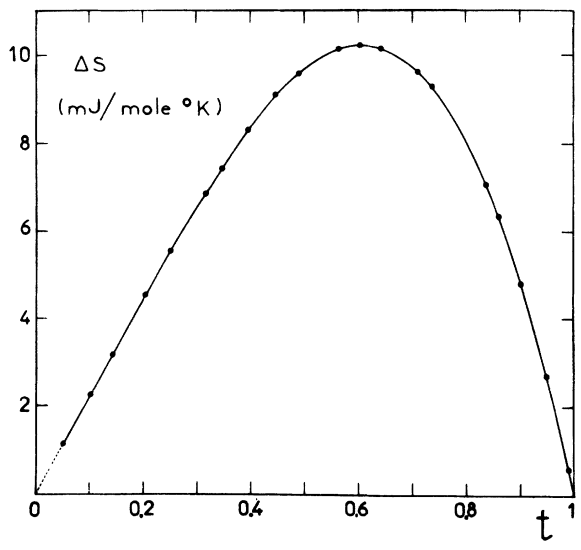


FIG. 4. Entropy difference vs reduced temperature $t$.

The normal-state electronic heat capacity may be expressed as $C_{en} = \gamma T$ and approaches the origin of Fig. 6 far more slowly than the superconductive component. Thus, the slope at the origin leads directly to $\gamma$

$$\gamma = \lim_{T \to 0} \frac{d}{dT} \Delta C = 3.13 \pm 0.06 \,(\mathrm{mJ/mole})^\circ \mathrm{K}^2 . \qquad (12)$$

We may now solve Eq. (11) for $C_{es}$. The result is shown in Fig. 7 as well as the BCS weak-coupling heat capacity.

## IV. CONCLUSION

### A. Critical-Field Curve

The curve of Fig. 2 shows the positive deviation from the parabolic temperature-dependence characteristic of strong-coupling superconductors. The position of the maximum deviation at $t = 0.66$, is identical with that found by Decker, Mapother, and Shaw[9] and the strong-coupling-theory calculation of Swihart, Scalopino, and Wada,[3] although the maximum deviation, +2.1%, is somewhat lower than their values of +2.4% and +2.7%, respectively. Our value of $T_c$ is in remarkable agreement with the measurement of Franck and Martin.[10] A resumé of our critical-field parameters and results of the thermodynamic analysis are compared with earlier investigations, both calorimetric and magnetic, in Table II.

### B. Thermodynamic Derivatives of the Critical-Field Curve

The quantities obtained by differentiation of the smoothed critical-field data in Sec. III may be compared with earlier magnetic and calorimetric investigations. The latent-heat curve is compared with the calorimetric measurement of Dolecek[11] in Fig. 5. From the $\Delta C$-vs-$T$ curve of Fig. 6,

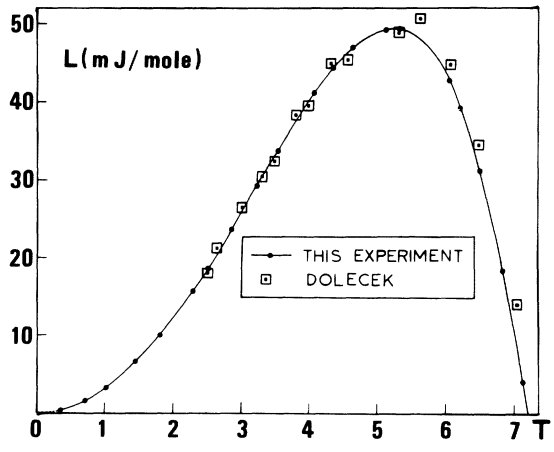


FIG. 5. Latent heat of transition vs absolute temperature $T$.

TABLE II. Summary of experimental measurements on lead. [(M) refers to magnetic measurements; (C) refers to calorimetric measurements.]

| | | $T_c$ (°K) | $H_0$ (Oe) | $\left.\frac{dH_c}{dT}\right\|_{T_c}$ (Oe/°K) | $\Delta C \mid_{T_c}$ (mJ/mole °K²) | $\gamma$ mJ/mole °K² | $C_{es}/\gamma T_c \mid_{T_c}$ |
|---|---|---|---|---|---|---|---|
| This experiment | (M) | 7.195 ± 0.006 | 803.4 ± 0.3 | −237.3 ± 1.1 | 59.9 ± 0.6 | 3.13 ± 0.06 | 3.6 |
| Decker, Mapother, and Shaw[a] | (M) | | 802.6 ± 0.4 | −238.4 ± 1.2 | 58.1 ± 0.7 | 3.06 ± 0.04 | 3.7 |
| Pedulla[b] | (M) | 7.236 ± 0.01 | 799.4 ± 0.8 | −231.3 | | 2.98 ± 0.08 | |
| Franck and Martin[c] | (M) | 7.193 ± 0.005 | | | | | |
| Pearson and Templeton[d] | (M) | 7.175 ± 0.005 | | | | | |
| Boorse, Cook, and Zemansky[e] | (M) | 7.22 ± 0.02 | | | | | |
| Neighbor, Cochran, and Shiffman[f] | (C) | | | | 58.5 ± 0.9 | | 3.71 |
| Van der Hoeven and Keesom[g] | (C) | | | | | 3.00 ± 0.04 | |
| Phillips, Lambert, and Gardner[h] | (C) | | | | | 3.00 | |
| Dolecek[i] | (C) | | | | | 3.35 | |
| Horowitz, Silvidi, Malaker, and Daunt[j] | (C) | | | | | 3.13 | |

[a] D. L. Decker, D. E. Mapother, and R. W. Shaw, Phys. Rev. 112, 1888 (1958).

[b] J. Pedulla, thesis, Master of Science (University of Pittsburgh, 1964) (unpublished).

[c] J. D. Franck and D. L. Martin, Can. J. Phys. 39, 1320 (1961).

[d] W. B. Pearson and I. M. Templeton, Phys. Rev. 109, 1094 (1958).

[e] H. A. Boorse, D. B. Cook, and M. W. Zemansky, Phys. Rev. 78, 635 (1950).

[f] J. E. Neighbor, T. F. Cochran, and C. A. Shiffman, Phys. Rev. 155, 384 (1967).

[g] J. C. Van der Hoeven, Jr., and P. H. Keesom, Phys. Rev. 137, A103 (1965).

[h] N. E. Phillips, M. H. Lambert, and W. R. Gardner, Rev. Mod. Phys. 36, 131 (1964).

[i] R. L. Dolecek, Phys. Rev. 94, 540 (1954).

[j] M. Horowitz, A. A. Silvidi, S. F. Malaker, and J. G. Daunt, Phys. Rev. 88, 1182 (1952).

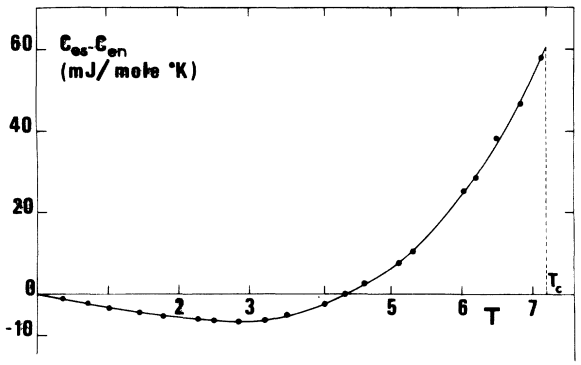


FIG. 6. Heat-capacity difference vs $T$.

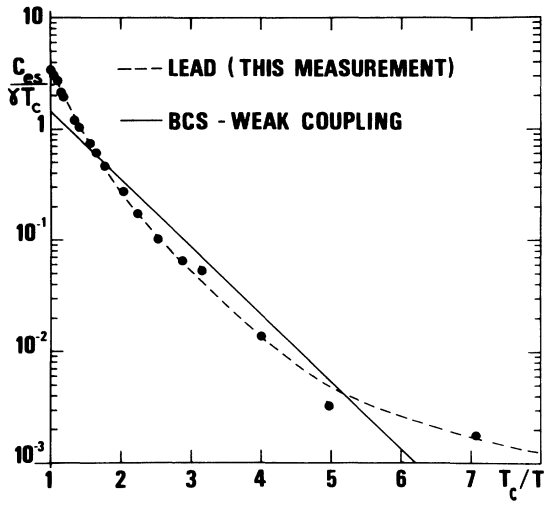


FIG. 7. $C_{es}/\gamma T_c$ vs $T_c/T$, the reciprocal reduced temperature.

the jump in heat capacity at the critical temperature $\Delta C|_{T_c}$ and the slope at the origin $\gamma$, were obtained. The comparison in Table II indicates that both are very slightly higher than earlier work. The curve of the superconductive electronic heat capacity (Fig. 7) is considerably above the BCS theory near the critical temperature. The value of the intercept in Table II, $(C_{es}/T_c)_{T_c}$, is seen to be in excellent agreement with earlier magnetic and calorimetric determinations. Since most superconductors also lie above the BCS curve near the origin, this is probably unrelated to the strong-coupling character of lead.

At low temperatures, the upward curvature persists, in agreement with Decker, Mapother, and Shaw[9] and the calorimetric determinations of Van de Hoeven and Keesom[12] rather than the much faster decrease of $C_{es}$ given by Neighbor, Cochran, and Shiffman.[18]

### C. Hysteresis and Phase-Boundary Mobility

The variation of hysteresis with temperature was indicated in Table I. Hysteresis values as low as 0.012% have been observed in the region around 4 °K proving that the phase boundary is at all times very near thermodynamic equilibrium with the applied field. Thermal excitation energies appear to be sufficient to overcome the attraction of surface imperfections and defects to "pin" the boundary in local regions of low surface energy. As this "pinning" would require magnetic forces to be built up before the boundary could be coerced to resume its displacement in response to the field scan, hysteresis would result. At low temperatures, such hysteresis occurs and appears to increase linearly with decreasing temperature (by an order of magnitude at the lowest temperatures). This effect is in qualitative agreement with the work of Decker, Mapother, and Shaw[9] but was not observed in earlier work in aluminum[2] using this same technique.

At temperatures very near $T_c$ a rapid increase with temperature in hysteresis was observed, in agreement with the earlier aluminum measurements.[2] This effect is perhaps related to the technique employed, since at low-field values, temperature and field stability become critical for the maintenance of boundary stability while at the same time the field regulation is decreasing. Occasionally, very low hysteresis values were also recorded as in Fig. 2. Further investigations of this effect in other metals will be useful in identifying its cause.

ACKNOWLEDGMENTS

We are pleased to acknowledge the aid of G. Le Rest, P. Vidit, and especially C. Plaisant for the construction and instrumentation of this apparatus.

---

†Parts of this paper are based upon a thesis submitted by J. P. Terre in partial fulfillment of the requirements for the Docteur Troisième Cycle degree, Université de Paris Sud, Centre d'Orsay, Orsay, 91, France.

[1]J. Bardeen, L. N. Cooper, and J. R. Schrieffer, Phys. Rev. 108, 1175 (1957).

[2]S. Caplan and G. Chanin, Phys. Rev. 138, A1428 (1965).

[3]J. C. Swihart, D. J. Scalopino, and Y. Wada, Phys. Rev. Letters 14, 106 (1965).

[4]G. Chanin, Cryogenics 10, 67 (1970).

[5]R. H. Sherman, T. R. Roberts, and S. G. Sydoriak, Report No. LAMS-2701, Los Alamos, 1962 (unpublished).

[6]F. G. Brickwedde, H. Van Dijk, M. Durieux, J. R. Clement, and J. K. Logan, J. Res. Natl. Bur. Std. 64A, 1 (1960).

[7]W. H. Keesom, *Helium* (Elsevier, Amsterdam, 1942), p. 49.

[8]T. R. Roberts and S. G. Sydoriak, Phys. Rev. 102, 304 (1956).
[9]D. L. Decker, D. E. Mapother, and R. W. Shaw, Phys. Rev. 112, 1888 (1958).
[10]J. D. Franck and D. L. Martin, Can. J. Phys. 39, 1320 (1961).
[11]R. L. Dolecek, Phys. Rev. 94, 540 (1954).
[12]J. C. Van der Hoeven, Jr. and P. H. Keesom, Phys. Rev. 137, A103 (1965).
[13]J. E. Neighbor, J. F. Cochran, and C. A. Shiffman, Phys. Rev. 155, 384 (1967).

PHYSICAL REVIEW B VOLUME 5, NUMBER 11 1 JUNE 1972

# Superconducting Energy Gap of Thorium Determined by Electron Tunneling*

B. A. Haskell, W. J. Keeler, † and D. K. Finnemore
*Institute for Atomic Research and Department of Physics, Iowa State University, Ames, Iowa* 50010
(Received 6 October 1971)

Electron-tunneling measurements have been performed over the temperature range 0.4–1.4 K on Th-$ThO_2$-Au tunnel junctions fabricated on the surface of polycrystalline thorium substrates. Both the temperature dependence of the energy gap and the voltage dependence of the tunneling density of states agree rather well with the theoretical predictions for a weak-coupling superconductor. No significant phonon-induced structure was observed in the tunneling density of states.

## I. INTRODUCTION

Transition-metal superconductors form a class of materials with widely varying properties, and as a class they are one of the least understood. Because their properties are dominated by the presence of *d* bands at the Fermi level, they frequently show characteristics which differ from those of the *s-p*-band superconductors.[1] In fact, it has been suggested that the fundamental mechanism responsible for superconductivity in these materials is different from that in the *s-p*-band materials.[2] Unfortunately, however, experimental work to confirm or refute this suggestion has been scarce because the superconducting properties of the transition metals are very sensitive to oxygen impurities and samples are difficult to prepare.

Early measurements for Ta and Nb [3] showed a well-behaved energy gap but high-quality tunnel junctions were more difficult to prepare than in the *s-p*-band superconductors. Attempts to prepare junctions by evaporation of the transition metal have been largely unsuccessful, but Shen[4] has shown that it is possible to obtain high-quality junctions by depositing a thin film of silver over a freshly cleaned and oxidized surface of bulk tantalum. One of his junctions showed less than 0.3% of the normal-state conductance in the region of the gap, and several also showed structure in the tunneling density of states at higher voltages which correlated well with the neutron-diffraction phonon density of states. Shen concluded that the electron-phonon interaction is the only mechanism needed to explain the superconducting properties of tantalum.

MacVicar[5] and Hafstrom and MacVicar[5] have used a similar method to prepare single-crystal niobium junctions, and find evidence for a highly anisotropic energy gap. They interpret their data in terms of the two-band model of Suhl, Matthias, and Walker[6] and suggest the presence of two distinct gaps in "clean" samples. For these cases, the magnitude of the energy gap associated with the *d* band is ten times the magnitude of the one associated with the *s* band. Similar measurements for rhenium[7] also show anisotropy but the magnitude is smaller than for Nb, less than 30%.

We have prepared Th-$ThO_2$-Au junctions by a method similar to that of Shen and report here the first electron-tunneling measurements of the energy gap of superconducting thorium. Results for polycrystalline samples show an excitation spectrum fairly close to the BCS[8] prediction.

## II. EXPERIMENTAL

Tunnel junctions were prepared on the surface of parallelepiped-shaped (1×12×12-mm) pieces of pure thorium which were provided by Peterson of the Ames Laboratory.[9] Spectroscopic analysis of the starting material showed that the main impurities were C and O at 46 and 122 ppm by weight, respectively. The most prevalent magnetic impurities were Cr, Mn, and Fe at levels less than 20, 20, and 6 ppm, respectively. To prepare the junction, the sample was mounted in a high-vacuum system and the surface was cleaned by electron bombardment from a hot tantalum filament. During